

# 撥水性パターニングにおける表面間力によるハジキ流動

宮本 公明\*

## Dewetting Flow Caused by Inter-surface Force during Hydrophobic Patterning

Kimiaki MIYAMOTO\*

### Abstract

Hydrophobic patterning is a method of precise patterning for printed electronics. Exposure to UV light is used to create wiring and electrode patterns on a pre-coated photo-polymer, then hydrophilic conductive ink makes the pattern according to the hydrophilicity induced by the UV light. This study clarifies effects of difference in inter-surface force of adjacent regions and effects of surface unevenness by solving a film profile equation. The results show that stripes of two different levels of hydrophobicity provide a sufficient condition to make a dewetting pattern. In other words, it is not necessary to combine the hydrophilic stripe with the hydrophobic stripe for creation of a dewetting pattern. Also, it was found that hydrophobicity in a hill of a wavy surface is better for quick dewetting. If this status is reversed, namely hydrophobicity in a valley on the surface, stabilization or slow dewetting is caused. These findings suggest that the capillary force and inter-surface force affect each other during dewetting when the thickness is in the sub-micron order and no gravity effect occurs to level the surface.

### 1. Introduction

Recent development of organic semi-conductors has enabled Thin Film Transistors (TFTs) to be fabricated using printing technology alone. Although many samples of printed TFTs have been exhibited at trade-shows, it is hard to start mass-production because of the printing accuracy required. Inkjet printing is preferable because it has flexible alignment features and allows printing TFTs on demand. However, the problem with IJ technology is the trade-off between productivity and drop size that is typically 10 microns. In contrast, the typical TFT requires a 5 micron gap between source and drain electrodes.

Photonic assistance or hydrophobic patterning was proposed to overcome the difference between IJ accuracy and requirements when printing TFTs<sup>1), 2)</sup>. This method changes the hydrophobic polymer surface allowing it to be wetted by hydrophilic IJ ink. A special hydrophobic polymer on a substrate is exposed to patterned UV light as shown in Fig. 1. Then its surface

changes to hydrophilic by a chemical decomposition. This reaction has the additional effect of shrinkage of polymer which combines the chemical pattern and physical pattern. When hydrophilic IJ ink is sprayed roughly on the hydrophilic part, the ink dewets the hydrophobic surface and concentrates at the hydrophilic part. Accuracy of this process depends on the dewetting behavior of the surface-ink system.

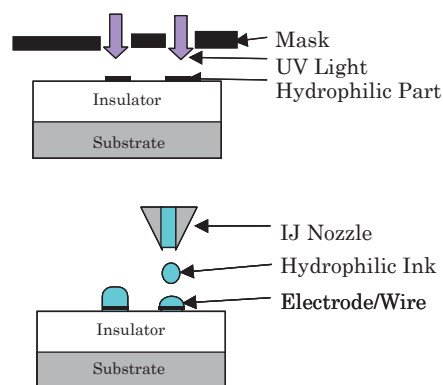


Fig. 1 Process of hydrophobic patterning.

本誌投稿論文（受理2012年10月26日）

\*富士フイルム（株）R&D統括本部

〒258-8577 神奈川県足柄上郡開成町牛島577

\*Research & Development Management Headquarters  
FUJIFILM Corporation  
Ushijima, Kaisei-machi, Ashigarakami-gun, Kanagawa  
258-8577, Japan

Intensive analysis of patterned dewetting was carried out by A. Sharma et al.<sup>3)~5)</sup>, but they limited cases to very thin film of fine patterns for use in the photo-lithography of semiconductor process. In the field of printed electronics, concerns are on much thicker film and a coarser pattern in the order of micrometers. This study elaborates on the dewetting phenomena found in the actual printed electronics process including the dewetting effect of solid surface morphology, Hamaker constant and liquid film parameters. The author adopts a theory by D. K. Owens and R. C. Wendt<sup>6)</sup> for the relationship between a contact angle and dispersion/non-dispersion components of both liquid and solid (eq. 1a-1c), which is an extension of the theory by Fowkes<sup>7)</sup>. Also the empirical relationship between surface energy components and the Hamaker constant is used according to A. Sharma and G. Reiter<sup>4)</sup> (eq. 2).

$$\gamma_i = \gamma_i^d + \gamma_i^h \quad (1a)$$

$$\gamma_{SL} = \gamma_S + \gamma_L - 2\sqrt{\gamma_S^d \gamma_L^d} - 2\sqrt{\gamma_S^h \gamma_L^h} \quad (1b)$$

$$1 + \cos \theta = 2\sqrt{\gamma_S^d} \left( \frac{\sqrt{\gamma_L^d}}{\gamma_L} \right) + 2\sqrt{\gamma_S^h} \left( \frac{\sqrt{\gamma_L^h}}{\gamma_L} \right) \quad (1c)$$

$$a_H = -24\pi d_0^2 \sqrt{\gamma_L^d} (\sqrt{\gamma_S^d} - \sqrt{\gamma_L^d}) \quad (2)$$

where  $\gamma_i$  is the surface energy of liquid L or solid S in [N/m],  $\gamma_i^d$  is the dispersion component of surface energy,  $\gamma_i^h$  is the non-dispersion component of surface energy and  $\theta$  is the contact angle.  $a_H$  is the Hamaker constant [J] of this system and  $d_0$  is the separation distance at contact [m].

This relationship supports the use of the Hamaker constant as a parameter for the disjoining pressure of a liquid-solid system (eq. 3). The flow driven by the disjoining pressure was analyzed earlier by M. B. Williams and S. H. Davis<sup>8)</sup> but the results were not precise enough. This study shows the results in greater detail with much more accuracy.

$$\Pi = \frac{a_H}{6\pi\delta^3} \quad (3)$$

where  $\Pi$  is the disjoining pressure [Pa],  $\delta$  is the liquid film thickness [m].

## 2. Model

The simplest model to examine the dewetting hydrodynamics is evenly coated liquid film on a flat surface with one half of the area hydrophilic and the other half hydrophobic as shown in Fig. 2.

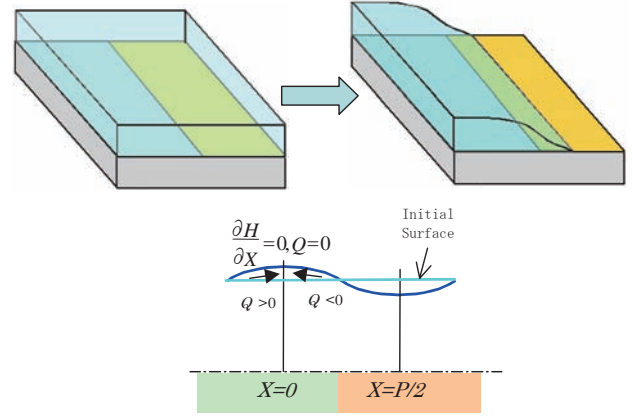


Fig. 2 Model for flat surface.

The boundary of these two regions is linear and a calculation domain corresponds to a half of the pitch of the line pattern. The well-known Film-Profile Equation (eq. 4) is used for calculation together with lubrication approximation.

$$\frac{\partial \delta}{\partial t} = -\frac{\partial q}{\partial x}, \quad \frac{\partial \delta}{\partial t} = \frac{\partial}{\partial x} \left[ \frac{\delta^3}{3} \left( \frac{\partial p}{\partial x} \right) \right] \quad (4)$$

where  $q$  is the unit width flow rate [m<sup>2</sup>/s],  $p$  is the total pressure in the liquid film [Pa].

Here, the pressure gradient includes not only the gravity potential term and capillary force term but also the gradient of a Hamaker constant and that of an inter-surface force.

(eq. 5) In the equation,  $\rho$  is the density [kg/m<sup>3</sup>],  $\sigma$  is the surface tension [N/m] and  $h$  is the surface position [m].

$$\frac{\partial p}{\partial x} = \rho g \frac{dh}{dx} - \sigma \frac{d^3 h}{dx^3} - \frac{1}{6\pi\delta^3} \frac{da_H}{dx} + \frac{a_H}{2\pi\delta^4} \frac{d\delta}{dx} \quad (5)$$

Coverage of this model is limited to calculation from the beginning of film thinning to the instant of film breakage at the thinnest point. Thus, the process of a receding contact line is not covered in this study.

Before solving the model numerically, the analytical relationship between a Hamaker constant and parameters is deduced. Dewetting flow stops when the capillary force balances with the inter-surface force

(eq. 6). Assuming that the film surface shape is a sinusoidal curve (Fig. 3), a simple equation expressing the parameter effect on the critical Hamaker constant is deduced. This shows that the Hamaker constant is proportional to the surface tension  $\sigma$  and the fourth power of the thickness  $\delta$ , and inversely proportional to the square of the pitch  $p_w$  (eq. 7). These findings are compared with numerical results in the next section.

$$\sigma \frac{d^3 h}{dx^3} \approx \frac{a_H}{2\pi\delta^4} \frac{d\delta}{dx} \quad (6)$$

$$a_H = -\frac{(2\pi)^3 \delta^4}{p_w^2} \sigma \quad (7)$$

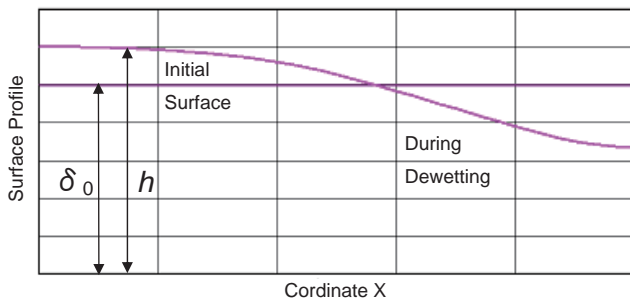


Fig. 3 Simple analytical model.

### 3. Parameter study by numerical calculation

Numerical analysis is performed with a flat surface, sinusoidal surface (eq. 8) and terrace surface (eq. 9).

$$h = \delta + h_0 = \delta - A_{mp} \cos(2\pi x / p_w) \quad (8)$$

$$h = \delta + h_0 = \delta + A_{mp} \tanh(\alpha(x - x_{orgn}) / \delta) \quad (9)$$

where  $A_{mp}$  is the amplitude of waviness [m],  $\alpha$  is the slope parameter [–] and  $h_0$  is the position of a solid surface [m].

With a terrace shape, polymer shrinkage by UV light and various line-and-space ratios are well demonstrated. Solutions are acquired by using the finite difference method and Euler integration with seven point expression of third order derivatives for better accuracy. Non-dimensionalization is performed by using the initial film thickness  $\delta_0$  as the length scale and  $\mu/\rho g \delta_0$  as the time scale. As a result, two non-dimensional parameters, the Bond number  $B_o$  and non-dimensional Hamaker constant  $A_H$ , are derived (eq. 10).

$$B_o = \frac{\rho g \delta_0^2}{\sigma}, \quad A_H = \frac{a_H}{\rho g \delta_0^2} \quad (10)$$

Basic parameters are 0.001 Pas for viscosity, 0.02 N/m for surface tension, 1,000 kg/m<sup>3</sup> for density, 0.1  $\mu$ m for

the liquid film thickness, 50  $\mu$ m for the pitch of a stripe and  $\pm 10\%$  difference in level between the steps of a terrace. Calculations are done with each value of the Hamaker constant (mostly negative) for the right half and with zero Hamaker constant for the left half in this parameter study section. Various combinations of Hamaker constants are investigated in the next section.

Two major phenomena, wetting and dewetting, are observed by the calculation (Fig. 4a, Fig. 4b). The dewetting case shows rapid thinning at the hydrophobic side creating zero thickness at the center of a hydrophobic stripe. There is a critical Hamaker constant that distinguishes between wetting and dewetting. In addition, strong dewetting may cause droplet formation resulting in incomplete dewetting with liquid left behind on the hydrophobic part (Fig. 4c).

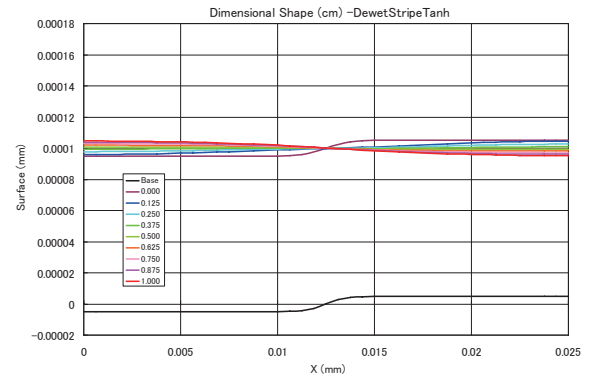


Fig. 4a Wetting.

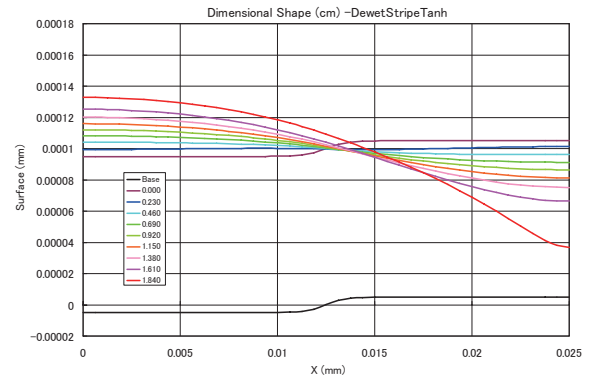


Fig. 4b Dewetting.

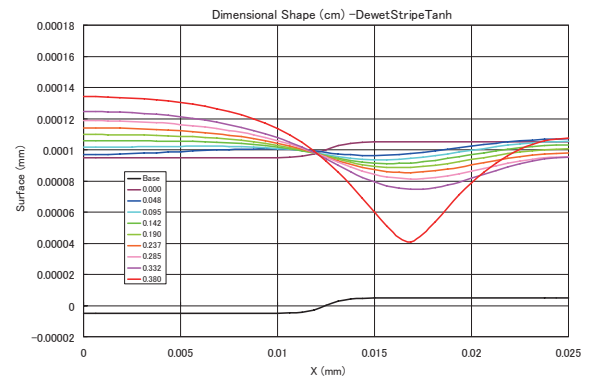


Fig. 4c Drop formation.

The hyperbolic tangent function is mainly used for a solid surface shape because this function can express a terrace shape that is commonly used in an actual printed electronics process (Fig. 5). A line-and-space ratio is usually not 1.0/1.0 because it depends on the circuit design, and a slope of the boundary between a hill and a valley varies depending on the defocus level of the UV light. These two surface morphology effects are examined first by changing parameters of the hyperbolic tangent function before calculating parameter effects. Fig. 6 shows the effect of the line-and-space ratio by shifting the origin of a hyperbolic tangent function together with a hydrophobic area that is on the right side of the origin of the curve. The vertical axis shows a negative critical Hamaker constant that distinguishes between wetting and dewetting, and the area above the graph line indicates dewetting resistance. The graph shows that the critical Hamaker constant changes slightly when the line-and-space ratio is changed from 12.5/37.5 to 37.5/12.5. Also the effect of slope is found to be weak as shown in Fig. 7.

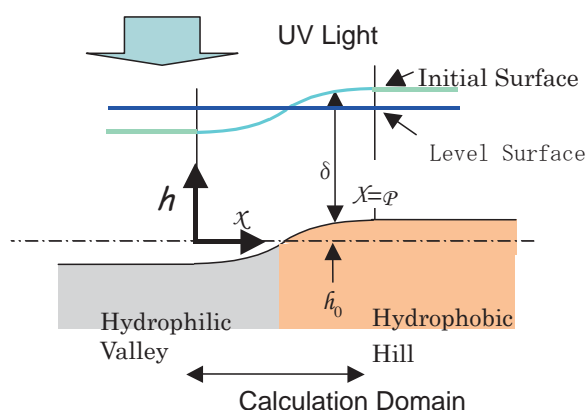


Fig. 5 Model for curved surface.

Therefore, the line-and-space ratio is fixed at 1.0/1.0 and a slope parameter of 0.1 is used in further sections.

The author examined the effects of solid surface shapes by using the shape function of flat, sinusoidal and hyperbolic tangent. The results for three surface shapes and an approximate solution are compared in Fig. 8 where the vertical axis also indicates a negative critical Hamaker constant. It is found that the surface waviness does not have much influence but it assists dewetting especially for shorter pitches. Waviness helps dewetting, which suggests a capillary force created by a curvature accelerates flattening and thinning the film toward dewetting at the beginning. However, the effect of shorter pitches, unlike the waviness effect, resists thinning in a later stage with a capillary force created by a concave surface. Also the graph shows that the simple analytical model represents a fair approximation of the numerical calculation for a flat surface. The comparison between the simple model and various parameter effects will be performed.

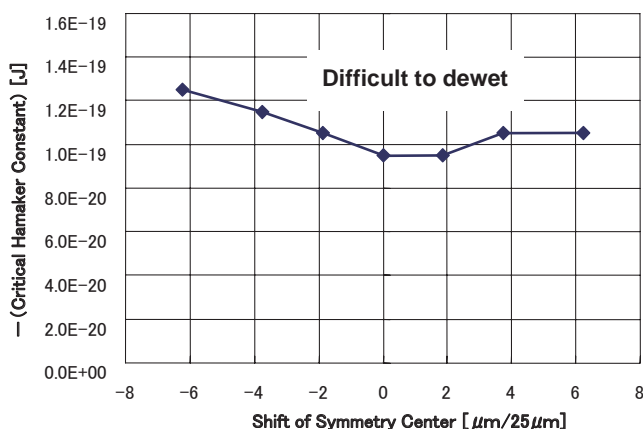


Fig. 6 Effect of line-and-space ratio on the critical Hamaker constant.

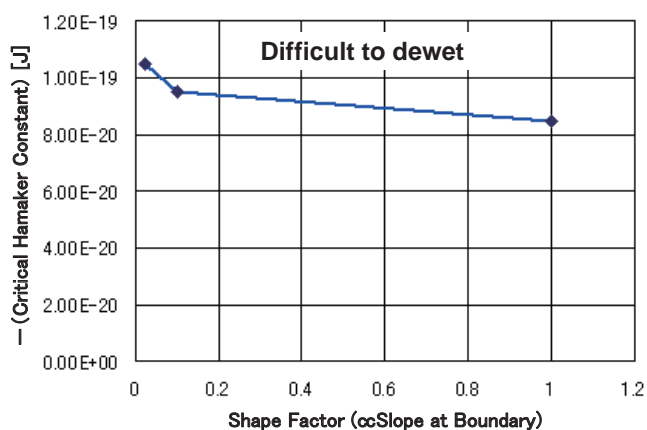


Fig. 7 Effect of slope at the boundary on the critical Hamaker constant.

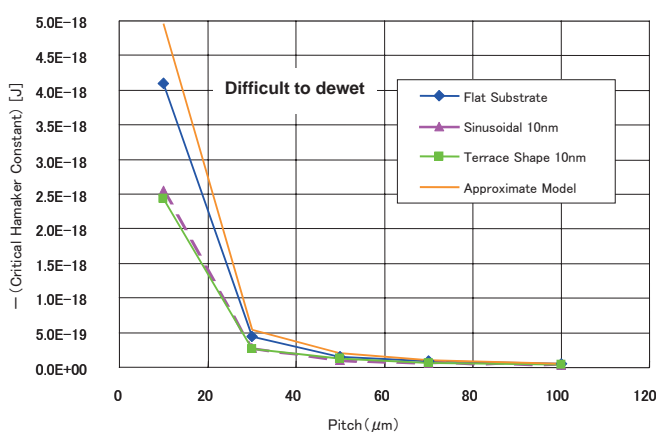


Fig. 8 Effect of pitch on the critical Hamaker constant.

Effects of liquid parameters are examined. The effect of viscosity is shown in Fig. 9 using the time length required for dewetting instead of a critical Hamaker constant as viscosity does not affect a critical Hamaker constant. This is because viscosity is only used in the non-dimensional time, not in the non-dimensional parameters in the differential equations. Therefore, the dewetting time required is linearly proportional to the degree of viscosity, which coincides with the empirical knowledge, “increase viscosity to prevent dewetting.”

The surface tension effect is examined, and in Fig. 10 the relationship between negative critical Hamaker constants and surface tension for various morphologies is shown. All the lines converge at the origin of the graph and dependence is linearly proportional to the surface tension. The effect of a pitch is shown together

with the surface tension effect. These effects can be reasonably explained by a hypothesis that the flattening effect of capillarity and the dewetting effect of hydrophobicity affect the level between each other. This mechanism is much different from the conventional theory, which solved the same equation, of film leveling caused by gravity and capillarity. The simple model result agrees with the numerical result for proportionality.

The effect of film thickness to the negative critical Hamaker constant is found to be proportional to 3.82 power of the thickness, which is slightly different from the analytical value of 4 (Fig. 11). The graph shows that there is no difference between the sinusoidal surface and terrace surface.

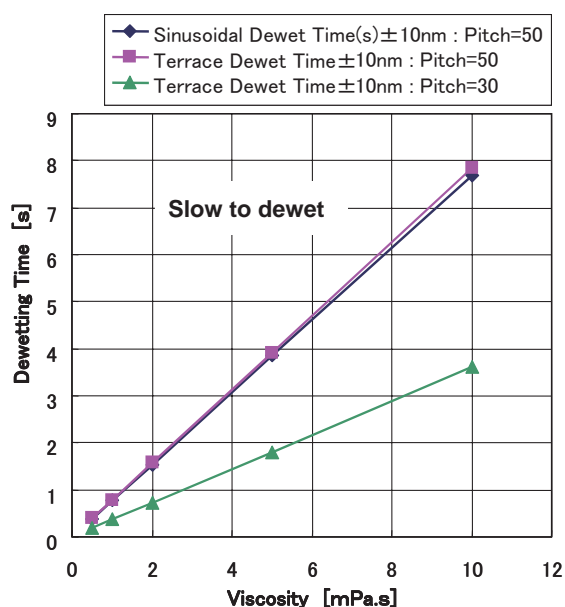


Fig. 9 Effect of viscosity on dewetting time.

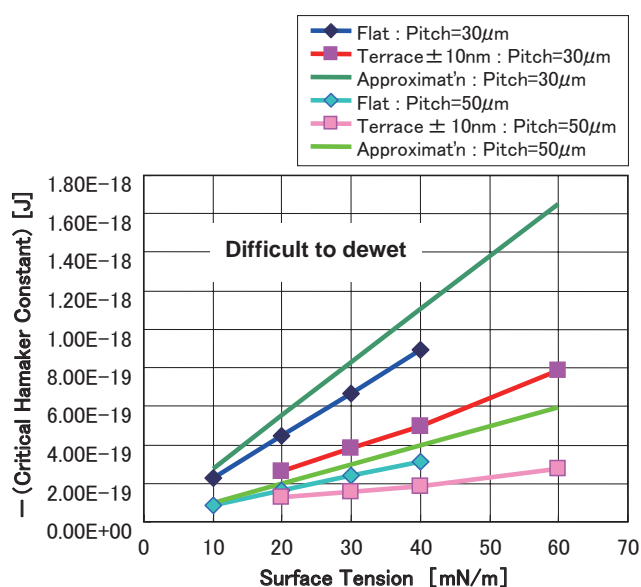


Fig. 10 Effect of surface tension on the critical Hamaker constant.

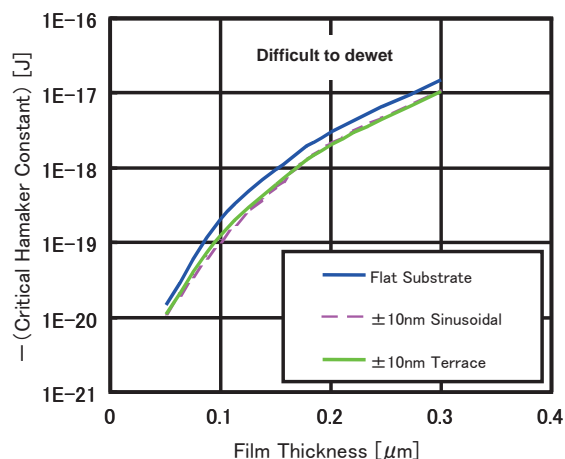


Fig. 11 Effect of film thickness on the critical Hamaker constant.



#### 4. Combination of two Hamaker constants for the hydrophobic area and hydrophilic area

There are various combinations of wettability of the hydrophilic area and the hydrophobic area in actual products. The result from the film on a combined surface with two Hamaker constants is of interest. Fig. 12, Fig. 13 and Fig. 14 visualize the dewettability of the film on a flat surface, sinusoidal surface and terrace shape surface. The horizontal axis corresponds to the Hamaker constant on the right side and the vertical axis corresponds to that on the left side. For a curved surface, the hill side is fixed to the right. In these figures, the left and/or bottom of axes represents the most hydrophobic condition. For the flat surface (Fig. 12), it is symmetric around the center so that the graph area is symmetric around the 45 degree line. It is found that

the liquid dewets when a Hamaker constant on the right side is more hydrophobic than  $-2 \times 10^{-19} \text{ J}$  even if the one on the left side is also hydrophobic, as long as the two constants are different. In other words, it is not necessary that a Hamaker constant on the left half to be positive. Another finding is incomplete dewetting that occurs with overly strong Hamaker constants. However, these strong Hamaker constants are difficult to attain in actual practice.

Fig. 13 shows the results of a sinusoidal surface, which is similar to the flat surface case except for the dewettability on the 45 degree line. As the system is no longer symmetric around the two-surface-boundary, the difference from flat cases appears even when two Hamaker constants are the same. Because the surface shape of a coated film has a curvature, capillary force is the initial driving force to flatten the surface, namely

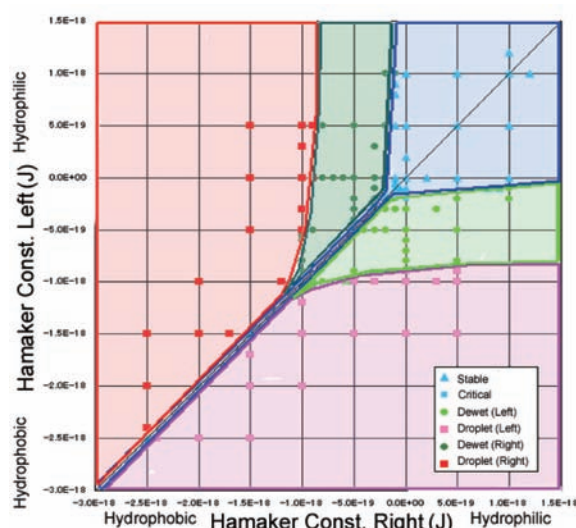


Fig. 12 Dewetting window for flat surface.

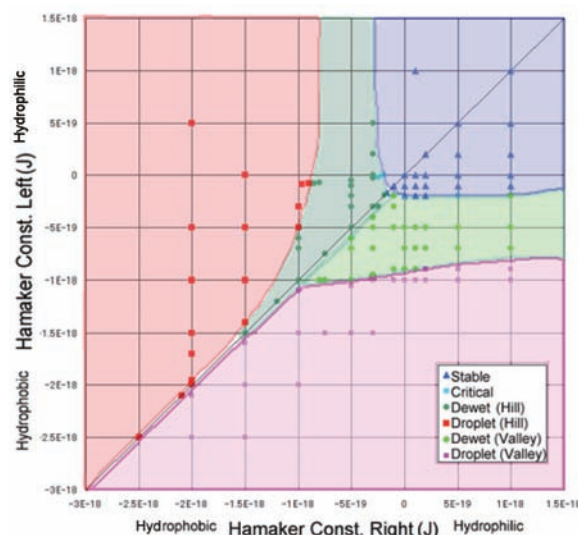


Fig. 13 Dewetting window for sinusoidal surface.

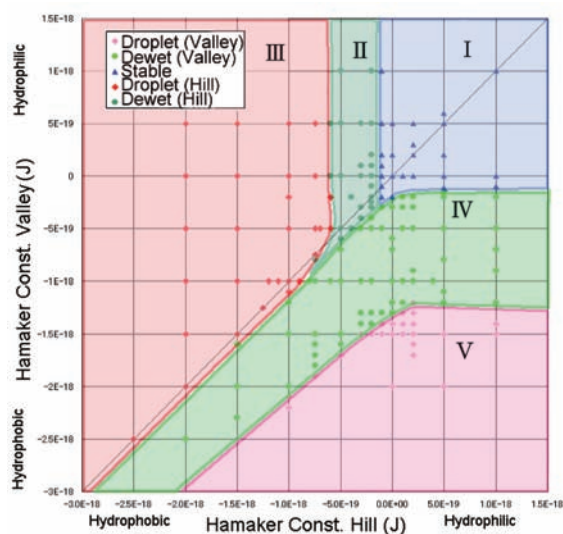


Fig. 14a (Top) Dewetting window for terrace shaped surface.

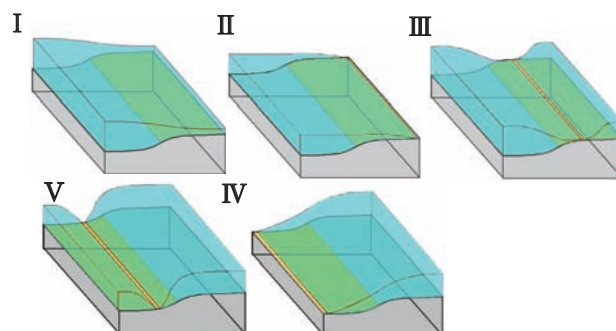


Fig. 14b (Bottom) Final shape of a liquid film.

to dewet, a pressure gradient with the same disjoining pressure at the boundary with the same Hamaker constants can be different at the point.

When the inter-surface force is strong enough, incomplete dewetting that forms droplets can also occur in the terrace surface case. The terrace shape case shown in Fig. 14 is basically similar to a flat surface case with the exception in the hydrophobic part at the valley of the terrace. In this case, hydrophobicity repels a liquid upward to the right hill although capillarity moves a liquid to the left valley, resulting in a very slow dewetting motion that might be the reason of complete dewetting free from drop formation. Finally, the author acknowledges that the weak effect of the surface shape appears to change the critical Hamaker constant to  $-1 \times 10^{-19} \text{J}$  from  $-2 \times 10^{-19} \text{J}$  for the flat surface.

## 5. Conclusion

The study of the dewetting process on hydrophobic and hydrophilic surfaces by changing parameters shows that the process is controlled by the mutual effects between the capillary and inter-surface forces. Also the results suggest that a large difference between the two Hamaker constants is not necessary but a reasonable hydrophobicity is necessary. The wider area of complete dewetting in Fig. 14 is a result of slower dewetting caused by hydrophobicity that moves the liquid against the opposing capillary force. Although these findings are helpful to find good conditions for dewetting, it is hard to estimate the practical Hamaker constants for actual systems. Future experimental confirmation of the theory is necessary for this study.

## References

- 1) Suzuki, K. et al. All-printed Organic TFT Backplanes for Flexible Electronic Paper. International Symposium on Electronic Paper 2010 (2010).
- 2) Maeda, H. Printed Organic TFT with High Operating Voltages for Active-Matrix Driven Electronic Papers. International Symposium on Electronic Paper 2010 (2010).
- 3) Sharma, A.; Jameel, A.T. Nonlinear Stability, Rupture, and Morphological Phase Separation of Thin Fluid Films on Apolar and Polar Substrates. *J. Coll. Interf. Sci.* **161**, 190-208 (1993).
- 4) Sharma, A.; Reiter, G. Instability on Thin Polymer Films on Coated Substrates: Rupture, Dewetting, and Drop Formation. *J. Coll. Interf. Sci.* **178**, 383-399 (1996).
- 5) Kargupta, K.; Sharma, A. Dewetting of Thin Films on Periodic Physically and Chemically Patterned Surfaces. *Langmuir*. **18**, 1893-1903 (2002).
- 6) Owens, D.K.; Wendt, R.C. Estimation of the Surface Free Energy of Polymers. *J. Appl. Polym. Sci.* **13**, 1741-1747 (1969).
- 7) Fowkes, F.M. ADDITIVITY OF INTERMOLECULAR FORCES AT INTERFACES. I. DETERMINATION OF THE CONTRIBUTION TO SURFACE AND INTERFACIAL TENSIONS OF DISPERSION FORCES IN VARIOUS LIQUIDS. *J. Phys. Chem.* **67**, 2538-2541 (1963).
- 8) Williams, M.; Davis, S.H. Nonlinear Theory of Film Rupture. *J. Coll. Interf. Sci.* **90**, 220-228 (1982).